

# Interpreting Black-box Machine Learning Models for High Dimensional Datasets

Md. Rezaul Karim<sup>†,\*</sup>, Md. Shajalal<sup>‡,\*</sup>, Alex Graß<sup>\*†</sup>, Till Döhmen<sup>\*,†</sup>, Sisay Adugna Chala<sup>\*,†</sup>,  
Christian Beecks<sup>\*§</sup>, Stefan Decker<sup>\*†</sup>

\* Fraunhofer Institute for Applied Information Technology FIT, Germany

† Information Systems and Databases, RWTH Aachen University, Germany

‡ University of Siegen, Germany

§ Chair of Data Science, University of Hagen, Germany

**Abstract**—Deep neural networks (DNNs) have shown to outperform traditional machine learning algorithms in a broad variety of application domains due to their effectiveness in modelling intricate problems and handling high dimensional datasets. Many real-life datasets, however, are of increasingly high dimensionality, where a large number of features maybe irrelevant for the task at hand. The inclusion of such features would not only introduce unwanted noise, but also increase computational complexity. Furthermore, due to high non-linearity and dependency among a large number of features, DNN models tend to be unavoidably opaque and perceived as *black-box* methods because of their not well-understood internal functioning. A well-interpretable model can identify statistically significant features and explain the way they affect the model's outcome. In this paper, we propose an efficient method to improve the interpretability of black-box models for classification tasks in case of high dimensional datasets. To this end, we first train a black-box model on a high dimensional dataset to learn the embeddings on which the classification is performed. To decompose the inner working principles of the black-box model and to identify top-k important features, we employ different probing and perturbing techniques. We then approximate the behavior of the black-box model by means of an interpretable *surrogate model* on the top-k feature space. Finally, we derive decision rules and local explanations from the surrogate model to explain individual decisions. Our approach outperforms and competes with state-of-the-art methods such as TabNet, XGboost, and SHAP-based interpretability techniques when tested on different datasets with varying dimensionality between 50 and 20,000.

**Index Terms**—Curse of dimensionality, Black-box models, Interpretability, Attention mechanism, Model surrogation.



## 1 INTRODUCTION

WITH high availability and easy access to large-scale data, high-performance hardware accelerators, state-of-the-art machine learning (ML) and deep neural networks (DNNs) algorithms, predictive modelling can now be performed at scale. However, in case of high dimensional datasets including images, omics, texts, or audio, the feature space (dimensionality) increases exponentially. In order to process such high-dimensional datasets, singular value decomposition (SVD)-based approaches such as principal component analysis (PCA) and isometric feature mapping (Isomap) have been extensively used in literature [1]. Although approaches based on PCA and Isomap found to be moderately effective dimensionality reduction methods that preserve inter-point distances, they are fundamentally limited to linear embedding and essential features are often lost [2]. This makes them less effective against phenomena like curse of dimensionality [1]. In contrast, DNNs have shown to benefit from higher pattern recognition capabilities when it comes to feature extraction. In particular, with multiple hidden layers and non-linear activation functions within each layer, autoencoder (AEs) architectures can learn to encode complex and higher-order feature interactions. Thus, the resultant embeddings can capture important contextual information of underlying data [3]. Further, learning non-linear mappings allows transforming and mapping input feature space into a lower-dimensional latent space, yielding downstream tasks-friendly representations [3].

However, due to high non-linearity and higher-order interactions among large number of features, DNN models are perceived as *black-box* methods because of non-transparent structure and internal functioning. For example, latent factors learned by AEs are not easily interpretable, whilst disentangling them can provide insight into what features are captured by the representations and what attributes of the samples the tasks are based on [3]. Nevertheless, a serious drawback is that predictions made by such a complex model can neither be traced back to the input, nor it is clear why outputs are transformed in a certain way by answering question such as “*how and why inputs are ultimately mapped to certain decisions*”. Further, in sensitive areas like high value financial trading, cybersecurity, and healthcare, where AI may has an impact on human lives, explainability and accountability are not only some desirable properties but also legal requirements [4], e.g., *EU GDPR* enforces that processing based on automated decision-making tools should be subject to suitable safeguards, including “*right to obtain an explanation of the decision reached after such assessment and to challenge the decision*”.

Since how a prediction is made by ML models should be as transparent as possible in a faithful and interpretable manner, model-specific and model-agnostic approaches covering local and global interpretability have emerged recently [5]. While local explanations focus on explaining individual predictions, global explanations explain entire model

behavior in the form of plots or more interpretable approximations such as decision sets or lists. Since interpretability comes at the cost of flexibility or efficiency, research has suggested for learning a simple interpretable model to imitate the complex black-box model globally and providing local explanations based on it [6]. Further, by representing the learned knowledge in a human-understandable way, an interpretable surrogate model’s input-output behaviour can help to better understand, explore, and validate the embedded knowledge [7]. In particular, decision rules containing *antecedents* (IF) and a *consequent* (THEN) are more effective at providing intuitive explanations compared to visualization-based explanations [6].

On the other hand, explanations that highlight the greatest difference between the object of interest and the reference object as the most user-friendly explanations [6]. Therefore, humans tend to think in a counterfactual way by asking questions like “how would the prediction have been if input  $x$  had been different?”. Therefore, by using a set of rules and counterfactuals, it is possible to explain decisions directly to humans with the ability to comprehend the underlying reason so that users can focus on understanding the learned knowledge without focusing much on the underlying data representations [7]. Mathematical certainty means it should be possible to transparently show that there is no hidden behaviour or logic influencing the behaviour of a model [8]. However, the inclusion of a large number of irrelevant features would not only introduce unwanted noise, but also increase computational complexity as the data tends to become sparser. With increased predictive modelling complexity involving even hundreds of relevant features and their interactions, making a general conclusion or interpreting black-box models outcome and their global behaviour becomes increasingly difficult, whereas many existing approaches do not take into account probing or understanding the inner structure of opaque models.

Considering these limitations, we propose a novel and efficient method to improve the interpretability of black-box models for classification tasks in case of high dimensional datasets. We train a black-box model on high dimensional datasets to learn the embeddings on which we perform the classification. Then, we apply probing and perturbing techniques and identify most important top-k features. An interpretable surrogate model is then built on the simplified feature space to approximate the behavior of the black-box. *Decision-rules* and *counterfactuals* are then extracted from the surrogate model. We hypothesize that: i) by decomposing the inner logic (e.g., what features the model put more attention to) of black-box, its opaqueness can be reduced by outlining most and least important features and ii) a representative decision rule set can be generated with the surrogate model, which can be used to sufficiently explain individual decisions in a human-interpretable way.

## 2 RELATED WORK

Existing interpretable ML methods can be categorized as either model-specific or model-agnostic with focus on local and global interpretability or either. The local interpretable model-agnostic explanations (LIME) [9], model understanding through subspace explanations (MUSE) [10], SHapley

Additive exPlanations [11] (SHAP and its variants kernel SHAP and tree SHAP), partial dependence plots (PDP), individual conditional expectation (ICE), permutation feature importance (PFI), and counterfactual explanations (CE) [5] are more widely used. These methods operate by approximating the outputs of an opaque ML model via tractable logic, such as game theoretic Shapley values (SVs) or local approximation via a linear model, thereby putting emphasis on the transparency and traceability of complex ML or black-box models [12].

However, these approaches do not take into account the inner structure of an opaque black-box model. Therefore, probing, perturbing, attention mechanism [17], sensitivity analysis (SA), saliency map, and gradient-based attribution methods have been proposed in order to understand the inner structure of complex models. Saliency map and gradient-based methods can identify relevant regions and assign importance to each input feature, e.g., pixel in an image, where first-order gradient information of a black-box model is used to produce maps indicating the relative importance of input features. Gradient-weighted class activation mapping (Grad-CAM++) [18] and layer-wise relevance propagation (LRP) [19] are examples of this category that highlight relevant parts of inputs, e.g., images to a DNN which caused the decision can be highlighted.

Attention mechanisms proposed to improve accuracy in a variety of supervised and language modelling tasks, as they can detect larger subsets of features. Self-attention network (SAN) [17] is proposed to identify important features from tabular data. TabNet [20] is proposed, which uses a sequential attention mechanism to choose a subset of semantically meaningful features to process at each decision step. It also visualizes the importance of features and how they are combined to quantify the contribution of each feature to the model enabling local and global interpretability. SAN is found effective on datasets having a large number of features, while its performance degrades in case of smaller datasets, indicating that having not enough data can distil the relevant parts of the feature space [17]. Since interpretability comes at cost of accuracy vs. complexity trade-off, research has suggested learning a simple interpretable model to imitate a complex model [6]. In particular, model interpretation strategy is used, which involves training an inherently interpretable *surrogate* model to learn a locally faithful approximation of the black-box model [6]. Since an explanation relates feature values of a sample to its prediction, rule-based explanations are easier to understand for humans [7]. Anchor [14] is a rule-based method that extends LIME, which provides explanations in the form of decision rules. Anchor computes rules by incrementally adding equality conditions in the antecedents, while an estimate of the rule precision is above a threshold [21].

However, a critical drawback of rule-based explanations could arise due to overlapping and contradictory rules. Sequential covering and Bayesian rule lists (BRL) are proposed to deal with these issues. Sequential covering iteratively learns a single rule covering the entire training data rule-by-rule, by removing the data points that are already covered by new rules [6], while SBRL combines pre-mined frequent patterns into a decision list using Bayesian statistics [6]. *Local rule-based explanations* (LORE) [21] is proposed to over-

TABLE 1: Approaches to interpretability of ML models based on agnosticism

Agnosticism	Global interpretability	Local interpretability
Model specific	Regression (logistic/linear) models	Individual (e.g., patient) specific set of decision rules
	Decision trees	Tree decomposition of decision rules
	Naïve Bayes	K-nearest neighbour (KNN)
	GNN Explainer [13]	GNN Explainer [13]
Model agnostic	Global surrogate models	Local interpretable model-agnostic explanation (LIME) [9]
	MUSE [10]	SHapley Additive exPlanations (SHAP) [11]
	Partial dependence plots (PDP)	Anchors [14]
	Summary plot with global feature importance	MUSE
	PFI [15]	CE [5]
	BETA [16]	Sailency and attention maps (e.g., CAM)

come these issues. LORE learns an interpretable model on a neighbourhood generated based on genetic algorithms. Then it derives local explanations from the interpretable model. Finally, it provides explanations in the form of a *decision rule*, and a set of *counterfactual rules* - that signifies making what feature values may lead to a different outcome. While LIME indicates where to look for a decision from categorical or continuous feature values, LORE’s counterfactual rules provide high-level and minimal-change contexts for reversing the outcome of a model. Although the explanations provided by LORE are more abstract than that of LIME and Anchors, it outperforms LIME and Anchor w.r.t. performance metrics.

### 3 PROPOSED APPROACH

This section outlines our proposed methods to interpret black-box models. First, we introduce several terminologies and notations that are used in the remainder of the paper.

**Definition 1 (Classifier).** Let  $\Theta$  be a set of parameters, where a parameter is a pair (*name, value*). A *classifier* is a parameterized function  $f : X \times \Theta \rightarrow \mathbb{R}$  that maps an input instance  $x$  from a feature space  $X$  to a decision  $y \in L$  and returns an output called *prediction*  $\hat{y}$ . A prediction  $\hat{y} = f(x_i, \theta)$  is accurate for model  $f$  and parameter  $\theta \in \Theta$  if and only if  $\hat{y} = \tilde{Y}[i]$  for  $x = \tilde{X}[i]$ , where  $1 \leq i \leq M$ .

**Definition 2 (Black-box and interpretable models).** Let  $f$  be a classifier.  $f$  is a black-box model if its internal working principle and parameters  $\theta$  are either hidden and unknown or known but uninterpretable by humans owing to lack of traceability how  $f$  makes predictions.  $f$  is interpretable if its parameters  $\theta$  are known to users and they have sufficient knowledge of how and why it generates certain predictions.

**Definition 3 (Feature importance).** Let  $a_i$  be a feature in instance  $x$ , and  $A$  be the set of all features. Importance function  $h : A \rightarrow [0, 1]$  assigns each element of  $A$  a non-negative number between 0 and 1: the larger the number, the higher the importance of  $a_i$ . Local feature importance for  $x$  is a set of feature and importance pairs  $I_x = \{(a_1, h(a_1)), (a_2, h(a_2)), \dots, (a_M, h(a_M))\}$  for all  $a_i \in x$ . Global feature importance for  $X$  is a set of feature and importance pairs  $\bar{I}_X = \{(a_1, \bar{p}_1), (a_2, \bar{p}_2), \dots, (a_k, \bar{p}_M)\}$ , where  $\bar{p}_i$  is the mean of all local feature importance of  $a_i$ .

**Definition 4 (Feature impact).** Let  $a_i$  be a feature of instance  $x$ , and  $A$  is the set of all feature names. Impact function

$g : A \rightarrow [-1, 1]$  takes an element of  $A$  as input and results in a real number between -1 and 1. Local feature impact for  $x$  is a set of feature and impact pairs  $T_x = \{(a_1, g(a_1)), (a_2, g(a_2)), \dots, (a_M, g(a_M))\}$  for all  $a_i \in x$ . Global feature impact for  $X$  is a set of feature and impact pairs  $\bar{T}_X = \{(a_1, \bar{q}_1), (a_2, \bar{q}_2), \dots, (a_k, \bar{q}_M)\}$ , where  $\bar{q}_i$  is the mean of all local feature impacts of feature for  $a_i$ .

**Definition 5 (Top-k and bottom-k features).** Let  $I$  be the global feature importance and  $k \in \mathbb{Z}^+$  be an integer. The top- $k$  features is a  $k$ -tuple such that for all  $i \leq k \leq m$ ,  $I[k[i]] \geq I[k[m+1]]$ , and  $I[k[i]] \geq I[k[i+1]]$ , where  $k$  is the number of top features to be picked to explain the decision. A bottom- $k$  features is a  $k$ -tuple such that for all  $i \geq k \geq m$ ,  $I[k[i]] \leq I[k[m+1]]$ , and  $I[k[i]] \leq I[k[i+1]]$ .

**Definition 6 (Decision rule).** A decision rule  $r$  is a formula  $p_1 \wedge p_2 \wedge \dots \wedge p_k \rightarrow y$ , where  $p_i$  are boolean conditions on feature values in instance  $x$  and  $\hat{y}$  is the decision. Each decision rule  $r$  is evaluated w.r.t a concrete instance  $x$  by replacing feature with feature value from  $x$ , and evaluating the boolean condition in the usual way and reaching a conclusion  $y$  if the condition evaluated to be true.

**Definition 7 (Counterfactual rules).** Let  $r : p \rightarrow y$  be a decision rule for an instance  $x$  and  $x'$  is the perturbed vector of  $x$  by applying  $w$ -perturbation<sup>1</sup>. A *counterfactual rule*  $r^\dagger$  for the boolean conditions  $p$  is a rule of the form  $r^\dagger : p[\delta] \rightarrow y'$  for  $y' = f(x')$  such that  $y' \neq y$ , where  $\delta$  is a *counterfactual* for original decision  $y = f(x)$  for model  $f$ .

**Definition 8 (Surrogate model).** Let  $x \in X$  be an instance of an  $m$ -tuple,  $Y$  be  $N$ -tuple of labels  $l \in L$ , and  $f_b$  be a black-box model. Model  $f$  is a *surrogate model* of  $f_b$  if the variance  $R^2$  (ref. eq. (13)) of  $f_b$  captured by  $f$  is  $\approx 1$ .

**Definition 9 (Interpretability).** *Interpretability* is the degree to which a human can understand the cause of a decision [12]. Global interpretability refers to an explanation  $e$  giving reasoning why model  $f$  has predicted  $\hat{y}$  for all instances in  $X$ , outlining overall conditional interactions between dependent- and independent variables using some functions  $\sigma(\cdot, \cdot)$ . Local interpretability reasons why model  $f$  has predicted  $\hat{y}$  for an instance  $x$ , outlining the conditional interaction between dependent variables and single prediction.

<sup>1</sup> A resulting vector by applying minimum change  $\Delta x$  to some feature values  $a_i$  using ADAM optimization method [5] s.t.  $y' = f(x')$  against original prediction  $y$ , where  $x' = x + \Delta x$ .  $x'$  is called a  $w$ -perturbation of  $x$  and  $y'$ .

**Definition 10 (Explanation).** An explanation  $e$  for a prediction  $\hat{y} = f(x)$  for an instance  $x \in X$  is an object derived from a classifier  $f$  using some function  $\sigma(\cdot, \cdot)$  that reasons over  $f$  and  $x$  for  $y$  such that  $e = \sigma(f, x)$  and  $e \in E$ , where  $E$  is the human-interpretable domain.

**Definition 11 (Local explanation).** Let  $f$  be a classifier,  $\hat{y} = f(x)$  be the prediction for instance  $x$ ,  $r$  be a decision rule for  $\hat{y}$ ,  $\Phi$  be the set of counterfactual rules for  $r$ , and  $I$  be the set of local feature importance for  $\hat{y}$ . A local explanation  $e$  explaining decision  $\hat{y}$  for  $x$  is a triple  $(I, r, \Phi)$ . The domain  $E_l$  of  $e$  is a  $N$ -tuple of triples  $(e_1, e_2, \dots, e_N)$ , where  $N$  is the number of instances in  $X$ .

**Definition 12 (Global explanation).** Let  $f$  be a classifier,  $\hat{y} = f(x)$  be the prediction for instance  $x$ ,  $\bar{I}$  and  $\bar{T}$  be the sets of global feature importances and impacts for all the predictions  $\hat{Y}$  for instances  $X$ ,  $\bar{I}_{k_t} = \{(a_1, \bar{q}_{1_t}), (a_2, \bar{q}_{2_t}), \dots, (a_k, \bar{q}_{k_t})\}$  be the set of top- $k$  features, and  $\bar{I}_{k_b} = \{(a_1, \bar{q}_{1_b}), (a_2, \bar{q}_{2_b}), \dots, (a_k, \bar{q}_{k_b})\}$  be the set of bottom- $k$  features. A global explanation  $e_g$  is a pair  $\langle \bar{I}_{k_t}, \bar{I}_{k_b} \rangle$ . The domain  $E_g$  of global explanation  $e_g$  is a pair  $(\bar{I}, \bar{T})$ .

### 3.1 Methods

The problem of classifying a set of instances is grouping them into specific classes, followed by explaining individual predictions. As outlined in fig. 1, a black-box model  $f_b$  is first trained on a high dimensional dataset to learn an embedding space that is used for classification. To decompose the inner principles of  $f_b$ , we apply probing and perturbing techniques and identify top- $k$  features w.r.t. feature impacts. An interpretable surrogate model  $f$  is then built on top- $k$  feature space to approximate the predictions of  $f_b$ . Finally, decision-rules are extracted and explanations are derived from  $f$  for each instance to explain individual decisions.

#### 3.1.1 Building black-box oracle model

We assume high dimensionality of each dataset, leading to a very large feature space  $|F|$ . We consider classifying instances into specific classes on the embedding space instead of their original feature space. Input  $X$  is first fed into a DNN to generate latent representations, thereby embedding the feature space into a lower dimensional latent space, s.t.  $X$  is transformed with a nonlinear mapping  $f_\Theta : X \rightarrow Z$ , where  $Z \in \mathbb{R}^K$  are the learned embeddings with  $K \ll F$ . A fully-connected softmax layer is added on top of DNN, thereby forming a black-box classifier  $f_b$ . To parameterize  $f_b$ , we train a convolutional autoencoder (CAE).

Due to function approximation properties and feature learning capabilities in CAE [22], deep and quality features can be easily extracted [3]. Further, since weights are shared, CAEs preserve locality and are able to better reduce the number of parameters in comparison to other AEs. A convolutional layer calculates the feature maps (FMs) on which max-pooling is performed to downsample them by taking the maximum value in each non-overlapping sub-region, thereby mapping and transforming  $X$  into a lower-dimensional embedding space  $Z$  [3]:

$$Z = g_\phi(X) = \sigma(W \odot X + b), \quad (1)$$

where encoder  $g(\cdot)$  is a sigmoid function parameterized by parameters  $\phi \in \Theta$  that include a weight matrix  $W \in \mathbb{R}^{p \times q}$  and a bias vector  $b \in \mathbb{R}^q$  in which  $p$  and  $q$  are numbers of input and hidden units,  $\odot$  is the convolutional operation,  $Z$  are the latent variables, and  $\sigma$  is the exponential linear unit activation function. The decoder function  $h(\cdot)$  reconstructs the original input  $X$  from latent representation  $Z$  by applying unpooling and deconvolution operations, such that  $Z$  is mapped back to a reconstructed version  $X' \approx X$  as follows [3]:

$$X' = h_\Theta(Z) = h_\Theta(g_\phi(X)), \quad (2)$$

where  $h(\cdot)$  is parameterized by  $(\theta, \phi) \in \Theta$  that are jointly learned to generate  $X'$ . This is analogous to learning an identity function, i.e.,  $X' \approx h_\theta(g_\phi(X))$ . Therefore,  $h_\theta(g_\phi(X))$  is equivalent to  $\Psi(W' * Z + b')$  [3]:

$$X' = \Psi(W' \odot Z + b'), \quad (3)$$

where  $\odot$  is the transposed convolution operation,  $W'$  is decoder's weights,  $b'$  is bias vectors, and  $\Psi$  is the sigmoid activation function. The unpooling is performed with switch variables [23] such that it remembers the positions of the maximum values during the max-pooling operation. Within each neighborhood of  $Z$ , both value and location of maximum elements are recorded: pooled maps store values, while switches record the locations. The mean squared error (MSE) is used to measure the reconstruction loss  $L_r$ :

$$L_r(\theta, \phi) = \frac{1}{N} \sum_{i=1}^N (X - X')^2 + \lambda \|W\|_2^2, \quad (4)$$

where  $\lambda$  is the activity regularizer and  $W$  are network weights. The latent vector  $Z$  is feed into a fully-connected softmax layer for the classification, which maps a latent point  $z_i$  into an output  $f_b(z_i) \mapsto \hat{y}_i$  in the embedding space  $Z$  by optimizing categorical cross-entropy (CE) loss (binary CE in case of binary classification) during back-propagation. The reconstruction loss and CE loss of CAE are combined and optimized jointly, during the backpropagation [3]:

$$L_{cae} = \sum_{i=1}^n \alpha_r L_r + \alpha_{ce} L_{ce}, \quad (5)$$

where  $\alpha_r$  and  $\alpha_{ce}$  are the regularization weights assigned to reconstruction and CE loss functions, respectively.

#### 3.1.2 Interpreting black-box models

We apply probing and perturbing techniques to interpret the black-box model.

3.1.2.1 Probing with attention mechanism: Figure 2 depicts an extended schematic representation of SAN architecture. The original SAN architecture that enables self-attention at the feature level can be represented as [17]:

$$l_2 = \sigma(W_2 \cdot (\alpha(W_{|F|} \cdot \Omega(X) + b_{l_1})) + b_{l_2}), \quad (6)$$

where  $\alpha$  is an activation function,  $b_{l_i}$  represents layer-wise bias, and  $\Omega$  represents the first network layer that maintains the connection with the input features  $X$  [17]:

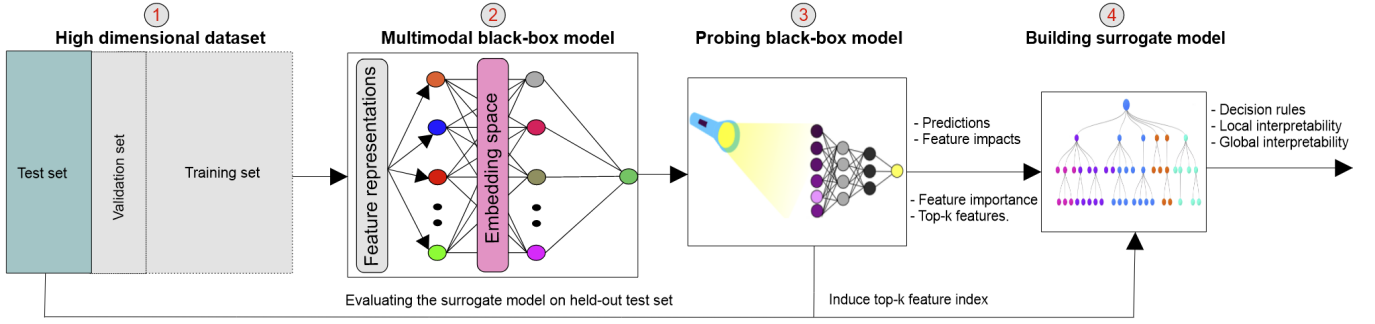


Fig. 1: Workflow of the proposed approach: gray circles with red numbers represent different steps of the process

$$\Omega(X) = \frac{1}{k} \bigoplus_k \left[ X \otimes \text{softmax} \left( W_{l_{\text{att}}}^k X + b_{l_{\text{att}}}^k \right) \right], \quad (7)$$

where  $X$  are first used as input to a softmax-activated layer by setting: i) its number of neurons equal to  $|F|$  and ii) number of attention heads representing relations between input features to  $k$ , and  $W_{l_{\text{att}}}^k$  represents a set of weights in individual attention heads. The softmax function applied to  $i$ -th element of a weight vector  $v$  is defined as follows [17]:

$$\text{softmax}(v_i) = \frac{\exp(v_i)}{\sum_{i=1}^{|F|} \exp(v_i)}, \quad (8)$$

where and  $W_{l_{\text{att}}}^k \in \mathbb{R}^{|F| \times |F|}$ ,  $v \in \mathbb{R}^{|F|}$ ,  $l_{\text{att}}$  represents the attention layer in which element-wise product with  $X$  is computed in the forward pass to predict labels  $\hat{y}$  of individual instances in which two consecutive dense layers  $l_1$  and  $l_2$  contribute to predictions,  $\otimes$  and  $\oplus$  are Hadamard product- and summation across  $k$  heads. As  $\Omega$  maintains a bijection between the set of features and attention head's weights, weights in the  $|F| \times |F|$  matrix represent the relations between features.

We hypothesize that a global attention weight vector can be generated by applying attention mechanism to encoder's bottleneck layer. This vector is then used to compute feature attributions. Unlike SAN, we apply attention to embedding space (encoder's deepest convolutional layer), which maintains the connection between latent features  $Z$  as follows:

$$\Omega(Z) = \frac{1}{k} \bigoplus_k \left[ Z \otimes \text{softmax} \left( W_{l_{\text{att}}}^k Z + b_{l_{\text{att}}}^k \right) \right]. \quad (9)$$

That is, embedding space  $Z$  is used as the input to the softmax layer in which number of neurons is equal to dimension of embedding space. The softmax function applied to  $i$ -th element of weight vector  $v_z$  as [17]:

$$\text{softmax}(v_{z_i}) = \frac{\exp(v_{z_i})}{\sum_{i=1}^{|Z|} \exp(v_{z_i})}; v_{z_i} \in \mathbb{R}^{|Z|} \quad (10)$$

Once the training is finished, weights of the attention layer's are activated using softmax activation as [24]:

$$R_l = \frac{1}{k} \bigoplus_k \left[ \text{softmax} \left( \text{diag} \left( W_{l_{\text{att}}}^k \right) \right) \right], \quad (11)$$

where  $W_{l_{\text{att}}}^k \in \mathbb{R}^{|Z| \times |Z|}$ . As the surrogate model is used to provide local explanations, top-k features are extracted as diagonal of  $W_{l_{\text{att}}}^k$  and ranked w.r.t. *feature importance*.

**3.1.2.2 Perturbing with sensitivity analysis:** We validate globally important features through SA with  $w$ -perturbations: we change a feature value by keeping other features unchanged. If a change of its value significantly impacts the prediction, the feature is considered to have (statistically) high impact on the prediction. We create a new set  $\hat{X}^*$  by applying  $w$ -perturbation over feature  $a_i$  and measure its sensitivity in global level. To measure the change in the predictions, we observe the MSE between actual and predicted labels and compare the probability distributions over the classes (for 2 most probable classes in a multiclass setting). The sensitivity  $S$  of a feature  $a_i$  is the difference of between the MSE values of original feature space  $X$  and sampled  $\hat{X}^*$ . However, since SA requires a large number of calculations (i.e.,  $N \times M$ ;  $N$  and  $M$  are the number of instances and features) across predictions, we make minimal changes by taking into consideration of only the top-k features, thereby reducing the computational complexity.

### 3.1.3 Model surrogation

Model surrogation is about approximating the predictive power of a black-box model. Since most important features are already identified by the black-box  $f_b$ , we hypothesize that training a surrogate model  $f$  on top-k feature space would be reasonable. We train  $f$  on sampled data  $X^*$  (simplified data containing important features only) and ground truths  $Y$  (see algorithm 1 in appendix). Further, since any interpretable model can be used for function  $g$  [6], we train decision trees (DT), random forest (RF), and extremely randomized trees (ERT) classifiers. DT iteratively splits  $X^*$  into multiple subsets w.r.t to threshold values of features at each node until each subset contains instances from one class only, where the relationship between a prediction  $\hat{y}_i^*$  and a feature  $a_i^*$  can be defined as follows [25]:

$$\hat{y}_i^* = f(a_i^*) = \sum_{j=1}^N c_j I \{a_i^* \in R_j\}, \quad (12)$$

where each sample  $x^*$  reaches exactly one leaf node,  $R_j$  is the subset of the data representing the combination of rules at each internal nodes, and  $I\{\cdot\}$  is an identity function [25]. The mean importance of a feature  $a_i$  is computed

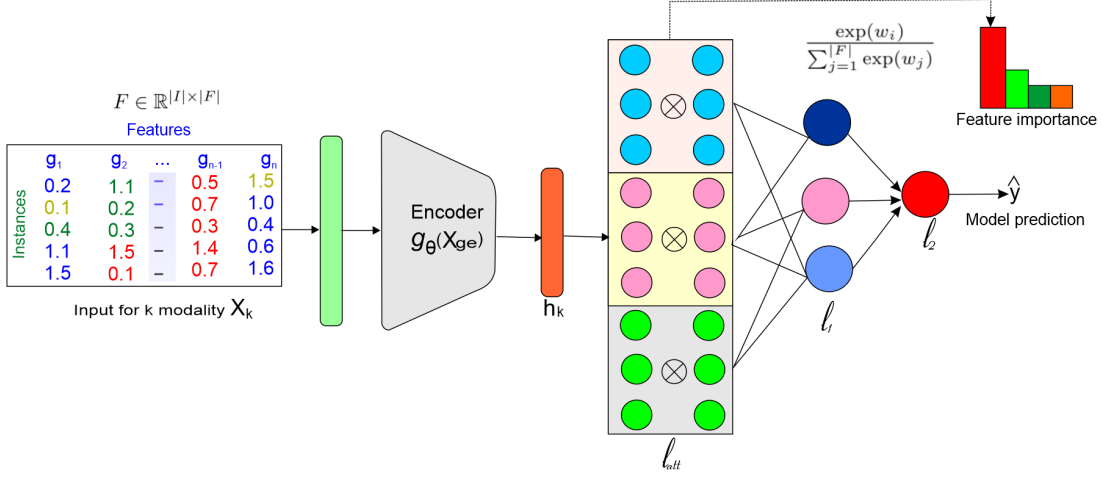


Fig. 2: Schematic representation of self-attention networks based on SAN [17]

by going through all the splits for which  $a_i$  was used and adding up how much it has improved the prediction in a child node (than its parent node) w.r.t decreased measure of Gini impurity  $I_{GQ} = \sum_{k=1}^N p_k \cdot (1 - p_k)$ , where  $p_k$  is the proportion of instances having label  $y_k^*$  in a node  $Q$ . The sum of all the values of importance is scaled to 1. The RF and ERT are trained to assemble randomized decisions to generate the final decision. Assuming the black-box  $f_b$  has sufficient knowledge, the *surrogate*, which has learned the mapping  $Y^* = f(X^*)$  is now able to mimic the model  $f_b$ .

---

#### Algorithm 1: Black-box model surrogation

---

**Input** : A simplified version  $X^*$  of dataset  $D^2$ , black-box model  $f_b$ , interpretable model type  $t$ , and model parameters  $\Theta^*$ .

**Output**: A surrogate model  $f$  and its predictions  $\hat{Y}_{test}^*$  on test set.

$X_{train}^*, Y_{train}^*, X_{test}^*, Y_{test}^* \leftarrow \text{TrainTestSplit}(X^*, Y)$

$X_{train}, Y_{train}, X_{test}, Y_{test} \leftarrow \text{TrainTestSplit}(X, Y)$

$cl_f \leftarrow \text{Estimator}(t, \Theta^*)$  // Create interpretable estimator

**for all batches in train set**  $\in X_{train}^*$  **do**

$f \leftarrow cl_f.\text{fit}(X_{train}^*, Y_{train}^*)$  // Train surrogate model

**return**  $f$

**end**

$M \leftarrow [f, f_b]$  // List of models, where  $f_b$  is trained on  $X_{train}$

**for model**  $\in M$  **do**

// Generate predictions

$\hat{Y}_{test} \leftarrow f_b.\text{predict}(X_{test})$  // for the black-box model

$\hat{Y}_{test}^* \leftarrow f.\text{predict}(X_{test}^*)$  // for the surrogate model

**return**  $\{f_b, \hat{Y}\}, \{f, \hat{Y}^*\}$

**end**

---

To measure how well  $f$  has replicated model  $f_b$ , R-squared measure ( $R^2$ ) is calculated as an indicator for

goodness-of-fit, which is conceptualized as the percentage of variance of  $f$  captured by the surrogate [6]:

$$R^2 = 1 - \frac{SSE^*}{SSE} = 1 - \frac{\sum_{i=1}^N (\hat{y}_i^* - \hat{y}_i)^2}{\sum_{i=1}^N (\hat{y}_i - \hat{y})^2}, \quad (13)$$

where  $\hat{y}_i^*$  is the prediction for  $f$ ,  $\hat{y}_i$  is the prediction for  $f_b$  for  $X^*$ , and  $SSE$  and  $SSE^*$  are the sum of squares errors for  $f$  and  $f_b$ , respectively [6]. Based on  $R^2$ , we decide if  $f$  can be used for real-life use case instead of  $f_b$  [6]:

- If  $R^2$  is close to 1 (low SSE), the surrogate model approximates the behavior of the black-box model very well. Hence,  $f_b$  can be used instead of  $f$ .
- If  $R^2$  is close to 0 (high SSE), the surrogate fails to approximate the black-box, hence cannot replace  $f_b$ .

#### 3.1.4 Deriving feature importance

First, we generate permutation feature importance (PFI) for  $f$ , which provides a view on global feature importance. However, since PFI does not necessarily reflect the intrinsic predictive value of a feature [26], features having lower importance for an under-/overfitted model could be important for a better-fitted model. Therefore, we employ SHAP to generate more consistent explanations. The SHAP importance for  $a_i \in x$  is computed using  $f$  by comparing what  $f$  predicts with and without it for all possible combinations of  $M-1$  features (i.e., except for  $a_i$ ) w.r.t SV  $\phi_i$  [26].

Since the order in which features are observed by the model matters, SVs explain the output of a function as the sum of effects  $\phi_i$  of each feature being observed into a conditional expectation. If  $a_i$  has zero effect on the prediction, it is expected to produce a SV of 0. If two features contribute equally, their SVs would be the same [11]. To compute global feature importance, absolute SVs per feature across all the training instances are averaged [26]. Further, to make the global feature importance consistent, we create stacking ensemble of SHAP values by averaging their marginal outputs of the SHAP values of DT, ERT, and RF models.

#### 3.1.5 Generating decision rules

We extract rule list  $R$  representing important rules for the surrogate  $f$ . As the decision rules can naturally be derived



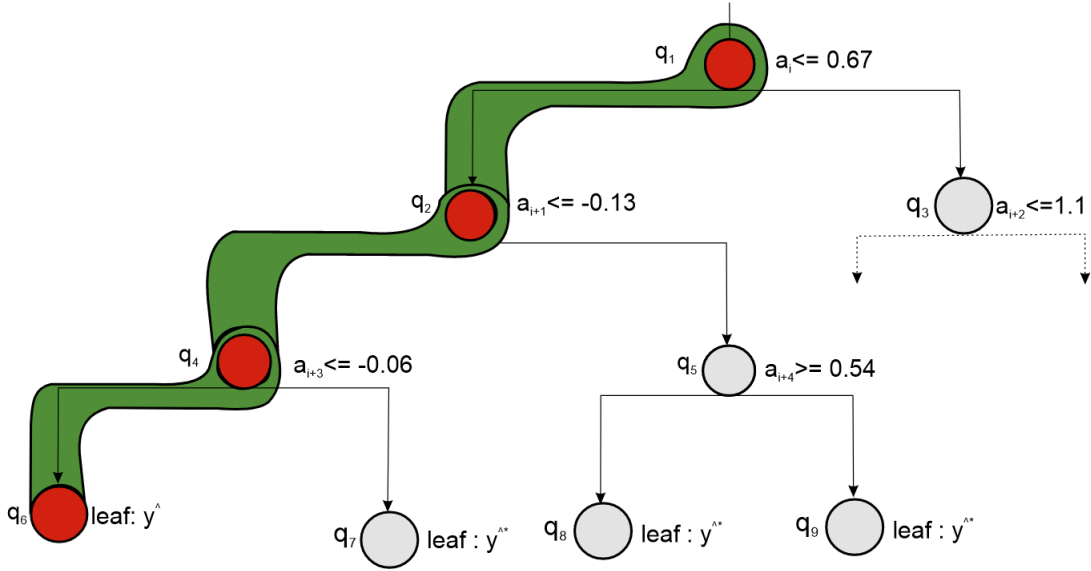


Fig. 3: Extraction of decision rules from a root-leaf path

from a root-leaf path in a DT to predict the class for an unseen instance [21], we follow the path of that instance down to the tree (as fig. 3 in supplementary). Starting at the root and satisfying the split condition of each decision node, we traverse until a leaf node is reached.

Unlike in a DT, a decision can be reached through multiple rules with excessive lengths. Considering the number of predictors, we apply representation of ordered list of inclusive rules based on SBRL in order to solve the issue of overlapping rules. Since the feature space is huge, textual representations would reduce human-interpretability – especially when the rule list length is large. Besides, some rules may not be useful in explaining individual decisions, e.g., rules having low confidence are insignificant in discriminating classes.

Therefore, we filter out rules that do not meet coverage, support, and confidence thresholds. Besides, we restrict the antecedents to be conjunction of clauses, i.e., each clause is a condition on feature  $a_i$ . The output of each rule is a probability distribution over the classes, i.e., the probability of an instance satisfying the antecedent belonging a class. Using SBRL, we combine pre-mined frequent patterns into a decision list [6]. The support of a pattern is measured as [6]:

$$\text{Support}(a_i) = \frac{1}{N} \sum_{i=1}^N I(a_i), \quad (14)$$

where  $I \in [0, 1]$ ,  $N$  is the number of data points and  $I$  is the indicator function that returns 1 if the feature  $a_i$  has level  $i$ , otherwise 0. Finally, the faithfulness of rules is computed w.r.t *coverage* that maximizes the fidelity of the rule list [7].

$$\text{fidelity}(R)_{X^*} = \frac{1}{|X^*|} \sum_{x^* \in X^*} [f(x^*) = R(x^*)], \quad (15)$$

where  $[f(x^*) = R(x^*)]$  returns 1 if  $f(x^*) = R(x^*)$ , 0 otherwise. Similar to [27], we generate counterfactuals by calculating the smallest possible changes ( $\Delta x$ ) to input  $x$  such that the outcome flips from original prediction  $y$  to  $y'$ .

## 4 EXPERIMENTS

We benchmark our approach on various datasets focusing on classification tasks. However, our approach is dataset-agnostic and can be applied to any tabular dataset. We implemented the methods in *Keras* and *PyTorch*. To provide fair comparison, we trained TabNet and XGBoost classifiers on same data as they are known to be effective for tabular datasets. Besides, we train MLP on PCA projection space. Isomap outperformed PCA-based projection for a number of tasks, even though it has computational complexity of  $O(n^3)$  [1]. Thus, we trained XGBoost on Isomap projection space. Adam optimizer and Glorot uniform initialization are used for training TabNet, MLP, and *SAN<sub>CAE</sub>* models whose hyperparameters were selected through 5-fold cross-validation and random search.

Each model is trained on 80% of data on Nvidia Quadro RTX 6000 GPU, followed by evaluating them on 20% held-out set. We provide qualitative and quantitative evaluations of each model, covering both local and global explanations. We report precision, recall, F1-score, and *Matthews correlation coefficient* (MCC) scores. We report  $R^2$  to quantitatively assess the predictive power of the surrogate models and support and fidelity to assess the quality of generated rules.

### 4.1 Datasets

We experimented on four datasets: i) gene expression (GE) dataset from the *Pan Cancer Atlas* project. This dataset covers 33 prevalent tumor types and has GE values of 20,531 features. It is widely used as a comprehensive source of omics data for cancer type prediction and tumor-specific biomarker discovery [28], ii) indoor localization dataset (UJIndoorLoc) [29] having 523 variables. This multi-building indoor localization dataset is used for indoor positioning systems based on WLAN/WiFi fingerprints, iii) *health advice* dataset [30] having 123 variables. This dataset was used to provide advice based on symptoms via a health-care chatbot, and ii) *forest cover type* dataset [31] having 54

TABLE 2: Sample distribution across tumor types

Cohort	#instances	Carcinoma type
ACC	227	Adrenocortical carcinoma
BLCA	71	Bladder urothelial carcinoma
BRCA	495	Breast invasive carcinoma
CESC	179	Cervical and endocervical cancers
CHOL	303	Cholangio carcinoma
COAD	96	Colon adenocarcinoma
DLBC	431	Lymphoid neoplasm diffuse large B-cell lymphom
ESCA	333	Esophageal carcinom
GBM	355	Glioblastoma multiforme
HNSC	581	Head and neck squamous cell carcinoma
KICH	817	Kidney chromophobe
KIRC	192	Kidney renal clear cell carcinoma
KIRP	179	Kidney renal papillary cell carcinoma
LAML	303	Acute myeloid Leukemia
LGG	96	Brain lower grade glioma
LIHC	431	Liver hepatocellular carcinoma
LUAD	333	Lung adenocarcinoma
LUSC	355	Lung squamous cell carcinoma
MESO	581	Mesothelioma
OV	817	Ovarian serous cystadenocarcinoma
PAAD	192	Pancreatic adenocarcinoma
PCPG	581	Pheochromocytoma and paraganglioma
PRAD	817	Prostate adenocarcinoma
READ	192	Rectum adenocarcinoma
SARC	179	Sarcoma
SKCM	303	Skin cutaneous melanoma
STAD	96	Stomach adenocarcinoma
TGCT	431	Testicular germ cell tumors
THCA	333	Thyroid carcinoma
THYM	355	Thymoma
UCEC	581	Uterine corpus endometrial carcinoma
UCS	817	Uterine carcinosarcoma
UVM	192	Uveal mlanoma

variables. This dataset is used for predicting forest cover type from cartographic variables.

This genomic data is hybridized with the Affymetrix Genome-Wide Human SNP Array 6.0, which allows us to examine the largest number of cases along with the highest probe density [32]. Sample distribution is shown in table 2.

## 4.2 Model performance analyses

We report the classification accuracy of each model w.r.t. increasing latent dimensions in fig. 4. When the projection dimension increases, the accuracy of each model also increases and the inter-model difference reduces, until a certain point where each model’s accuracy tends to decrease again. Since embedding smaller dimensional datasets into much low dimensions tend to lose essential information to correctly classify data points, it results in significant performance degradation, e.g., in case of health advice and forest cover type datasets, the classification accuracy improves up to  $45 \approx 55\%$  projected dimension only.

In case of very high dimensional datasets (e.g., GE and UJIndoorLoc), projecting them into embedding space with  $5 \approx 7\%$  dimension not to lose much information necessary to classify the data points. It is likely that higher dimensions bring more noise than information, making the classification task harder and no better than baseline (beyond 5% for the GE and 9% for the UJIndoorLoc dataset).

We report the performance of individual models in table 3. Asymptotically,  $MLP_{PCA}$  model consistently yielded the lowest accuracy across all the dataset, while  $XGBoost_{Isomap}$  slightly outperformed  $MLP_{PCA}$ . As PCA features are projected onto the orthogonal basis, they are linearly uncorrelated and similar to a single layered AE with a linear activation function. Eventhough Isomap can learn a

TABLE 3: Performance of individual models

Classifier	Dataset	Precision	Recall	F1	MCC
$MLP_{PCA}$	Gene expression	0.7745	0.7637	0.7553	0.7367
	UJIndoorLoc	0.8652	0.8543	0.8437	0.7741
	Health advice	0.8743	0.8679	0.8564	0.8067
	Cover type	0.7654	0.7547	0.7522	0.7126
$XGBoost$	Gene expression	0.8725	0.8623	0.8532	0.7851
	UJIndoorLoc	0.8964	0.8931	0.8836	0.7959
	Health advice	0.9354	0.9301	0.9155	0.8211
	Cover type	0.8382	0.8265	0.8184	0.7963
TabNet	Gene expression	0.9326	0.9276	0.9175	0.8221
	UJIndoorLoc	0.9217	0.9105	0.9072	0.8051
	Health advice	0.9455	0.9317	0.9178	0.8235
	Cover type	0.8953	0.8879	0.8854	0.8057
$SAN_{CAE}$	Gene expression	0.9525	0.9442	0.9325	0.8353
	UJIndoorLoc	0.9357	0.9269	0.9175	0.8233
	Health advice	0.9623	0.9538	0.9329	0.8451
	Cover type	0.9112	0.9105	0.9023	0.8124

projection that preserves the intrinsic structure of the data, it is not able to grasp non-linearity, hence failed to learn complex transformations.  $SAN_{CAE}$  and  $TabNet$  yielded comparable accuracy as both architectures learn projections that preserves relevant information for the classification. However,  $SAN_{CAE}$  outperformed  $TabNet$  as CAE modeled non-linear interactions among large number of features and generate classification-friendly representations.

The precision plot outlines the relationship between predicted probability (that an index belongs to the positive) and the percentage of the observed index in the positive class. The observations get binned together in groups of roughly equal predicted probabilities, and the percentage of positives is calculated for each bin. Further, we provided the decision boundary (i.e., a hyper-surface that partitions underlying vector space) by partitioning underlying vector space (given that showing so many different classes, e.g, 33 classes for GE and 42 for the symptoms precaution datasets in a single decision space is difficult) for each classifier in fig. 10. Each classifier classifies data points on one side of the decision boundary as belonging to one class and all those on the other side as belonging to the other class.

To analyse the reason, we provide precision plot and lift curve for the GE dataset (ref. figures 6 and 7 in supplementary). As observed from the precision plot, the fraction of positive increases with the predicted probability. While a perfectly calibrated model would show a straight line from the bottom left corner to the top right corner, a better-fitted model would classify most observations correctly with close to 100% probability. Thus,  $SAN_{CAE}$  model would make more reliable predictions (ref. precision and recall scores of 9 in supplementary), giving a precision score of 0.968. The lift curve shows the percentage of positive classes when observations with a score above the cutoff are selected vs. random selection. The  $SAN_{CAE}$  model identifies 95 observations accurately out of 100 (ref. confusion matrix of fig. 5 in supplementary), whereas only 17 observations are correctly predicted when done with random selection.

## 4.3 Performance of surrogate models

The fidelity and confidence of rule sets on test sets are demonstrated in table 4. The mean fidelity is shown in percentage and the standard deviations (SDs) for 5 runs are provided as  $\pm$ . Fidelity levels of 80%, 60% to 80%, and below 60% are considered as high, medium, and low, respectively.



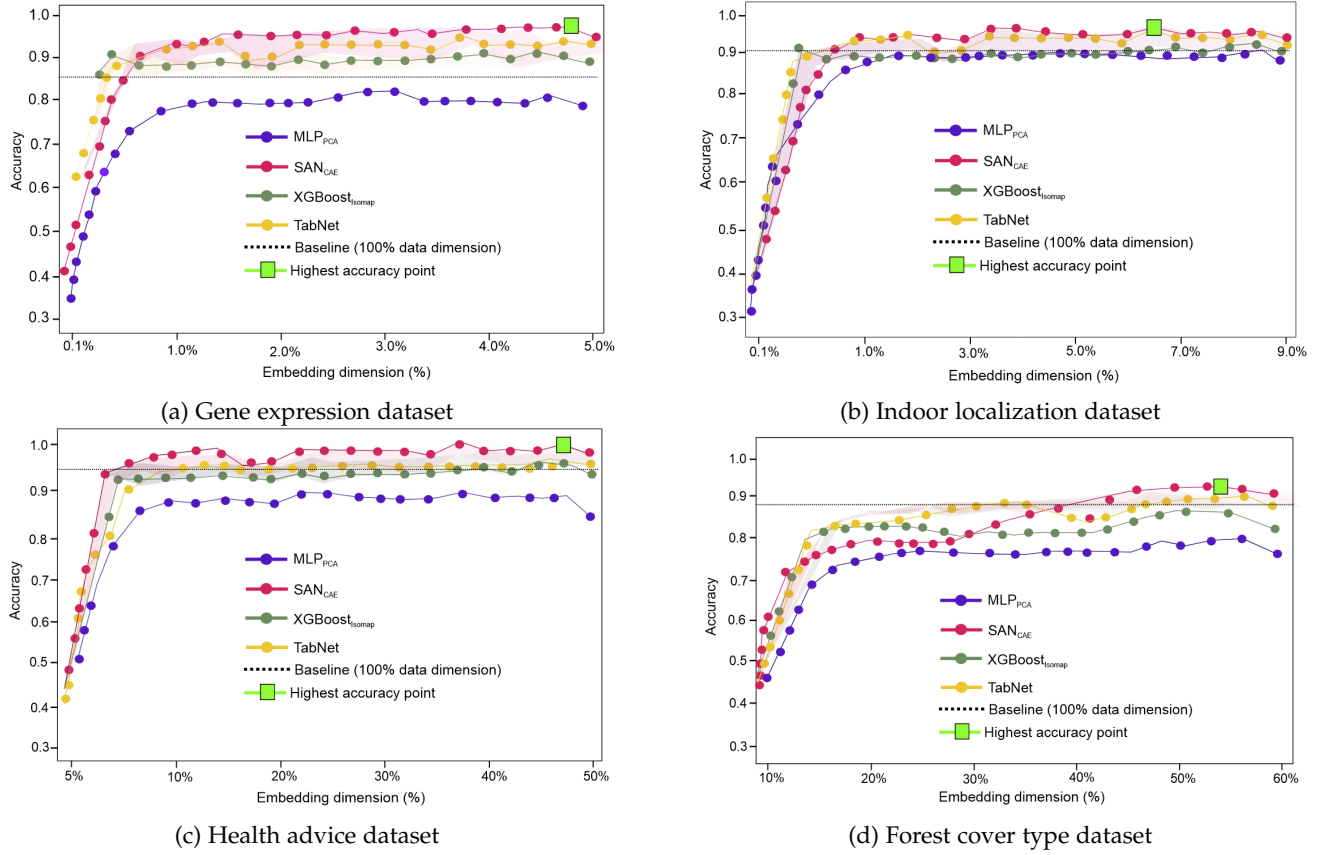


Fig. 4: Mean accuracy w.r.t the relative dimension of latent space. The shade indicates the standard deviation. The baseline is obtained by training the *TabNet* model on the original feature space (i.e., 100% of the dimensions)

TABLE 4: Fidelity vs. confidence of rule sets for the surrogate models

Dataset	DT		RF		ERT	
	Fidelity	Confidence	Fidelity	Confidence	Fidelity	Confidence
UJIndoorLoc	86.16 ± 1.72	85.37 ± 1.53	89.27 ± 1.46	88.11 ± 1.21	90.25 ± 1.38	<b>89.15 ± 1.57</b>
Health advice	88.35 ± 1.45	87.55 ± 1.85	90.11 ± 1.81	89.45 ± 1.35	91.38 ± 1.65	<b>90.25 ± 1.42</b>
Forest cover type	90.23 ± 1.37	88.75 ± 1.32	93.15 ± 1.42	91.25 ± 1.31	94.36 ± 1.35	<b>92.17 ± 1.34</b>
Gene expression	91.27 ± 1.42	89.33 ± 1.25	92.25 ± 1.35	90.21 ± 1.29	93.45 ± 1.25	<b>91.37 ± 1.35</b>

TABLE 5: Mean variance of surrogate models

Dataset	$R^2$ (DT)	$R^2$ (RF)	$R^2$ (ERT)
UJIndoorLoc	86.16 ± 1.72	89.27 ± 1.46	<b>91.35 ± 1.55</b>
Symptom precaution	89.35 ± 1.45	92.11 ± 1.8	<b>94.15 ± 1.75</b>
Forest cover type	90.23 ± 1.37	91.15 ± 1.4	<b>94.35 ± 1.25</b>
Gene expression	88.25 ± 1.42	90.23 ± 1.35	<b>93.27 ± 1.55</b>

As of *UJIndoorLoc*, ERT model achieved the highest fidelity and confidence scores of 90.25% and 89.15%, with the SDs of 1.38% and 1.57%. RF model also performed moderately well giving the second highest fidelity and confidence of 88.11% and 90.25%, with SDs of 1.21% and 1.38%. As of *health advice*, ERT model achieved the highest fidelity and confidence of 91.38% and 90.25%, with the SDs of 1.65% and 1.42%, respectively. The RF model also performed moderately well giving second highest fidelity and confidence of 90.11% and 89.45%, with slightly lower SDs of 1.81% and 1.35%.

As of *forest cover type*, ERT model achieved the highest fidelity and confidence of 94.36% and 92.17%, with the SDs of 1.35% and 1.34%. The RF model also performed moderately well giving second highest fidelity and confidence of 93.15% and 91.25%, with slightly lower SDs of 1.42% and 1.31%. As

of *gene expression*, ERT model achieved the highest fidelity and confidence of 93.45% and 91.37%, with the SDs of 1.25% and 1.35%. The RF model also performed moderately well giving second highest fidelity and confidence of 92.25% and 90.21%, with slightly lower SDs of 1.35% and 1.29%.

The percentage of variance ( $R^2$ ) for the surrogate models are shown in table 5. It turns out that  $R^2$  for the ERT model is comparable to the best performing *SAN<sub>CAE</sub>* and *TabNet* models. A surrogate model that largely approximates the predictive power of a complex black-box model can be reused with some sacrifice in accuracies.

#### 4.4 Global interpretability

We argue that providing both global and local explanations for all the datasets will be overwhelming and due to page restrictions. Therefore, we focus on the gene expression dataset only. Accurate identification of most and least significant features help understand various aspects such as their relevance w.r.t certain predictions or classes. For example, biologically relevant genes w.r.t specific cancer types provide insights into carcinogenesis as they could be viewed as potential biomarkers. Therefore, global feature



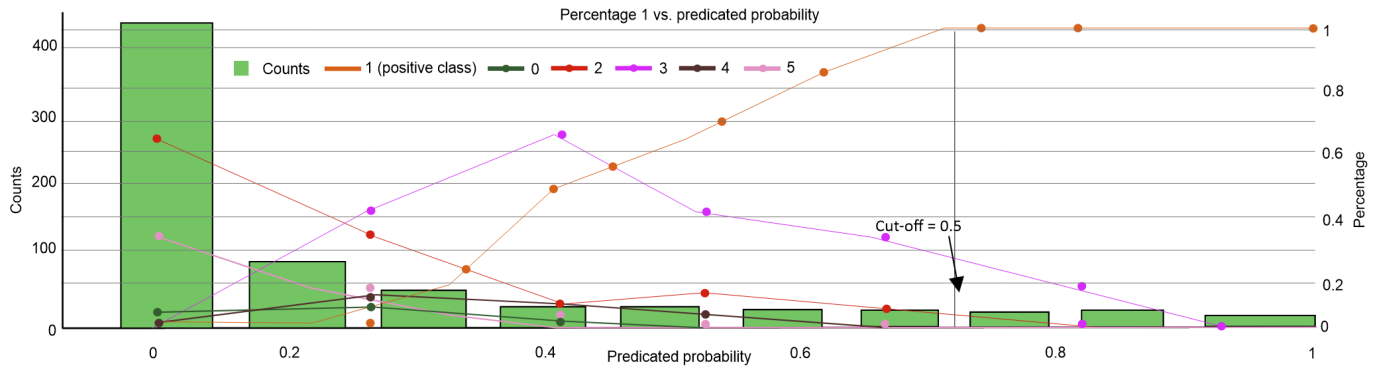


Fig. 6: Precision plot: if the fraction positive increases with the predicted probability

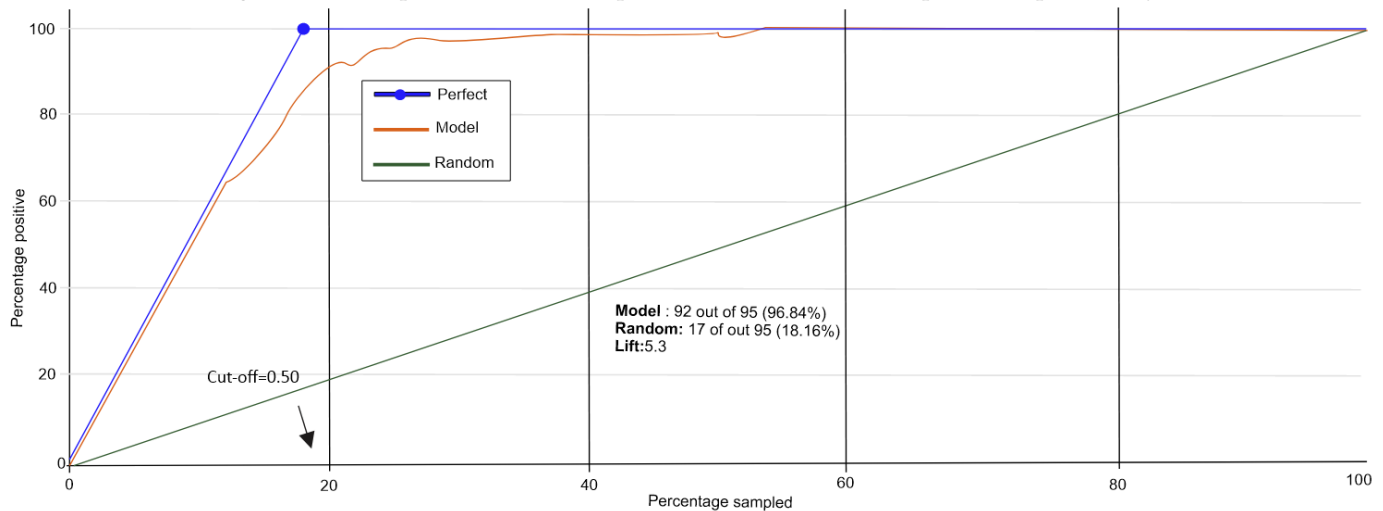


Fig. 7: Lift curve: the percentage of positive classes when observations with a score above cutoff is selected vs. random

Fig. 8: Precision plot and lift curve for the  $SAN_{CAE}$  model trained on GE dataset

tures on the left negatively. Genes TFAP2A, VPS9D1-AS1, MTND2P28, ADCY3, FOXP4, GPRIN1, EFNB1, FABP4, MGP, AC020916-1, CDC7, CHADL, RPL10P6, OASL, and PRSS16 are most sensitive to making changes, while features SEMA4C, CWH43, HAGLROS, SEMA3E, and IVL are less sensitive to making changes. However, if we remove feature TFAP2A from the profile, we would expect the model to predict the observation to be of COAD cancer type with a probability of 26% (i.e., 55% – 29%). This will recourse the actual prediction to BRCA in which features IVL, PRSS16, EFNB1, and CWH43 are most important, having impacts of 0.23, 0.17, 0.123, and 0.07, respectively. These features not only reveal their relevance for this decision, but also signify that removing them is like to impact the final prediction.

Further, we focus on local explanations for this prediction by connecting *decision rules* and counterfactuals with additive feature attributions (AFA) in fig. 15. While Anchor provides a single rule outlining which features impacted at arriving this decision, LIME generates AFA stating which features had positive and negative impacts. However, using decision rules and a set of counterfactuals, we show how the classifier could arrive at the same decision in multiple ways due to different negative or positive feature impacts.

## REFERENCES

- [1] Q. Fournier and D. Aloise, "Empirical comparison between autoencoders and traditional dimensionality reduction methods," in *2019 IEEE Second International Conference on Artificial Intelligence and Knowledge Engineering (AIKE)*. IEEE, 2019, pp. 211–214.
- [2] C. C. Aggarwal and C. K. Reddy, *Data clustering: algorithms and applications*. CRC press, 2014.
- [3] M. R. Karim, O. Beyan, A. Zappa, I. G. Costa, D. Rebholz-Schuhmann, M. Cochez, and S. Decker, "Deep learning-based clustering approaches for bioinformatics," *Briefings in Bioinformatics*, 02 2020.
- [4] M. E. Kaminski, "The right to explanation, explained," *Berkeley Tech. LJ*, vol. 34, p. 189, 2019.
- [5] S. Wachter, B. Mittelstadt, and C. Russell, "Counterfactual explanations without opening the black box: Automated decisions and the GDPR," *Harv. JL & Tech.*, vol. 31, p. 841, 2017.
- [6] C. Molnar, *Interpretable machine learning*. Lulu.com, 2020.
- [7] Y. Ming, H. Qu, and E. Bertini, "RuleMatrix: Visualizing and understanding classifiers with rules," *IEEE transactions on visualization and computer graphics*, vol. 25, no. 1, pp. 342–352, 2018.
- [8] C. Molnar, *Interpretable machine learning*. Lulu.com, 2019.
- [9] M. Ribeiro, S. Singh, and C. Guestrin, "Local interpretable model-agnostic explanations (LIME): An introduction," 2019.
- [10] H. Lakkaraju, E. Kamar, R. Caruana, and J. Leskovec, "Faithful and customizable explanations of black box models," in *Proceedings of AAAI/ACM Conference on AI, Ethics, and Society*, 2019, pp. 131–138.
- [11] S. M. Lundberg and S.-I. Lee, "A unified approach to interpreting model predictions," in *Advances in neural information processing systems*, 2017, pp. 4765–4774.
- [12] T. Miller, "Explanation in artificial intelligence: Insights from the social sciences," *Artificial Intelligence*, 2018.

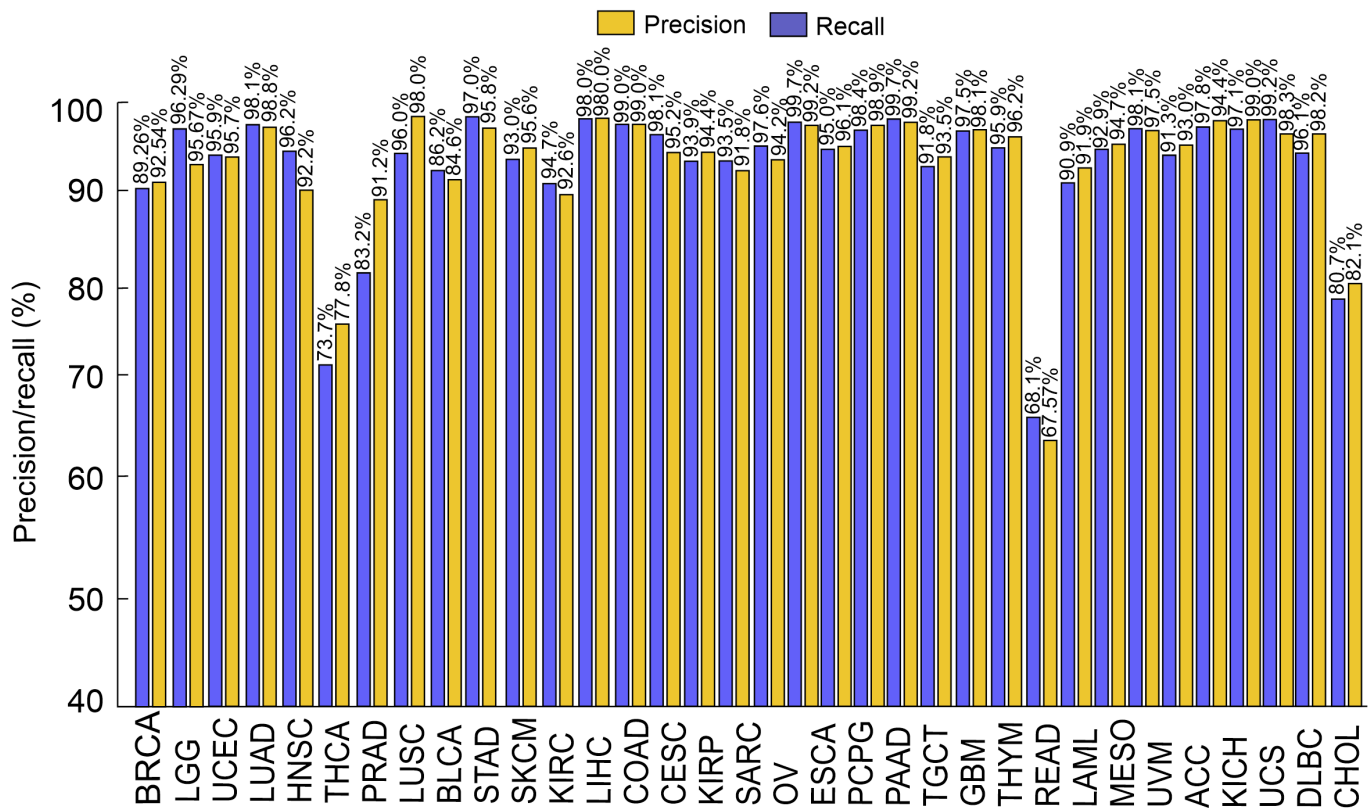
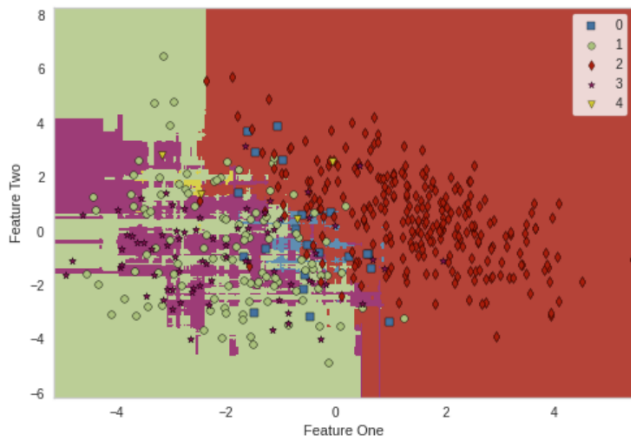
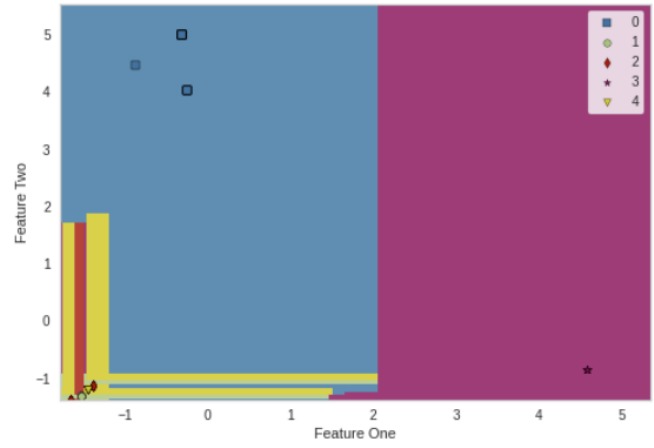


Fig. 9: Precision (blue) and recall (yellow) scores for the  $SAN_{CAE}$  model

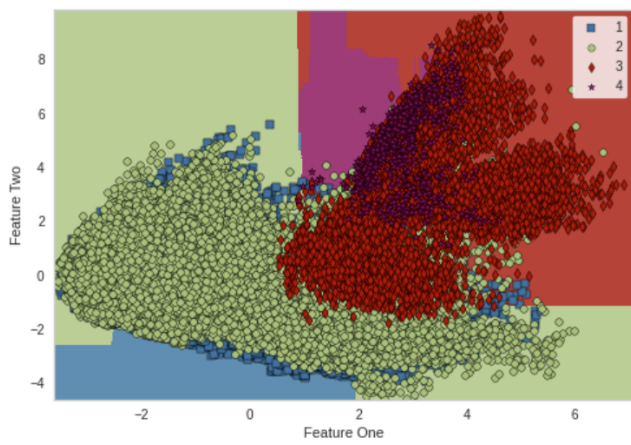
- [13] R. Ying, D. Bourgeois, J. You, M. Zitnik, and J. Leskovec, "GNN explainer: A tool for post-hoc explanation of graph neural networks," *arXiv preprint arXiv:1903.03894*, 2019.
- [14] M. T. Ribeiro, S. Singh, and C. Guestrin, "Anchors: High-precision model-agnostic explanations," in *Thirty-Second AAAI Conference on Artificial Intelligence*, 2018.
- [15] A. Fisher, C. Rudin, and F. Dominici, "Model class reliance: Variable importance measures for any machine learning model class, from the "rashomon" perspective," *arXiv preprint arXiv:1801.01489*, vol. 68, 2018.
- [16] H. Lakkaraju, E. Kamar, R. Caruana, and J. Leskovec, "Interpretable & explorable approximations of black box models," *arXiv preprint arXiv:1707.01154*, 2017.
- [17] B. Škrlj, S. Džeroski, N. Lavrač, and M. Petkovič, "Feature importance estimation with self-attention networks," *arXiv preprint arXiv:2002.04464*, 2020.
- [18] A. Chattopadhyay and A. Sarkar, "Grad-CAM++: Generalized gradient-based visual explanations for deep convolutional networks," in *Conf. on Applications of Computer Vision(WACV)*. IEEE, 2018, pp. 839–847.
- [19] S. Bach, A. Binder, G. Montavon, K.-R. Müller, and W. Samek, "On pixel-wise explanations for non-linear classifier decisions by layer-wise relevance propagation," *PloS one*, vol. 10, no. 7, 2015.
- [20] S. O. Arık and T. Pfister, "TabNet: Attentive interpretable tabular learning," in *AAAI*, vol. 35, 2021, pp. 6679–6687.
- [21] R. Guidotti, A. Monreale, S. Ruggieri, D. Pedreschi, F. Turini, and F. Giannotti, "Local rule-based explanations of black box decision systems," *arXiv preprint arXiv:1805.10820*, 2018.
- [22] J. Xie, R. Girshick, and A. Farhadi, "Unsupervised deep embedding for clustering analysis," in *International conference on machine learning*. New York City, NY, USA: ICMLR, 2016, pp. 478–487.
- [23] M. D. Zeiler, G. W. Taylor, and R. Fergus, "Adaptive deconvolutional networks for mid and high level feature learning," in *2011 international conference on computer vision*. IEEE, 2011, pp. 2018–2025.
- [24] A. Vaswani, N. Shazeer, N. Parmar, J. Uszkoreit, L. Jones, A. N. Gomez, Ł. Kaiser, and I. Polosukhin, "Attention is all you need," *Advances in neural information processing systems*, vol. 30, pp. 5998–6008, 2017.
- [25] F. Di Castro and E. Bertini, "Surrogate decision tree visualization." in *ILUI Workshops*, 2019.
- [26] S. M. Lundberg and S.-I. Lee, "Consistent feature attribution for tree ensembles," *arXiv preprint arXiv:1706.06060*, 2017.
- [27] R. M. Grath, L. Costabello, C. L. Van, P. Sweeney, F. Kamiab, Z. Shen, and F. Lecue, "Interpretable credit application predictions with counterfactual explanations," *arXiv preprint arXiv:1811.05245*, 2018.
- [28] K. A. Hoadley, C. Yau, T. Hinoue, D. M. Wolf, A. J. Lazar, E. Drill, R. Shen, A. M. Taylor, A. D. Cherniack, V. Thorsson *et al.*, "Cell-of-origin patterns dominate the molecular classification of 10,000 tumors from 33 types of cancer," *Cell*, vol. 173, no. 2, pp. 291–304, 2018.
- [29] J. Torres-Sospedra, R. Montoliu, A. Martínez-Usó, T. J. Arnau, M. Benedito-Bordonau, and J. Huerta, "Ujiindoorloc: A new multi-building and multi-floor database for wlan fingerprint-based indoor localization problems," in *2014 international conference on indoor positioning and indoor navigation (IPIN)*. IEEE, 2014, pp. 261–270.
- [30] P. Patil, "Healthcare chatbot," <https://github.com/itachi9604/healthcare-chatbot>, 2020.
- [31] J. A. Blackard and D. J. Dean, "Comparative accuracies of artificial neural networks and discriminant analysis in predicting forest cover types from cartographic variables," *Computers and electronics in agriculture*, vol. 24, no. 3, pp. 131–151, 1999.
- [32] R. W. Park and *et al.*, "Identification of rare germline copy number variations over-represented in five human cancer types," *Molecular cancer*, vol. 14(1), p. 25, 2015.



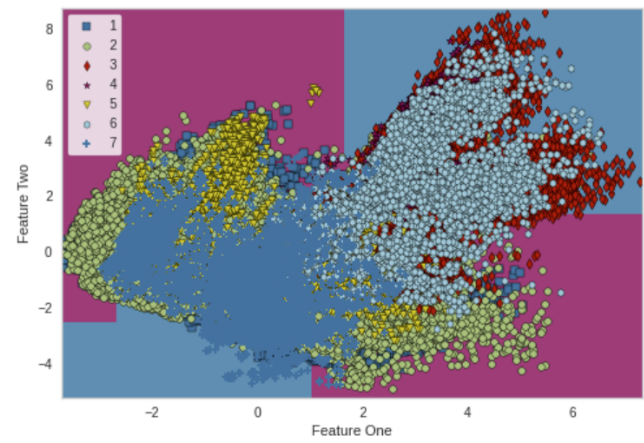
(a) Gene expression



(b) UJIndoorLoc



(c) Symptom precaution



(d) Forest cover type

Fig. 10: ERT's decision boundaries for top-2 features



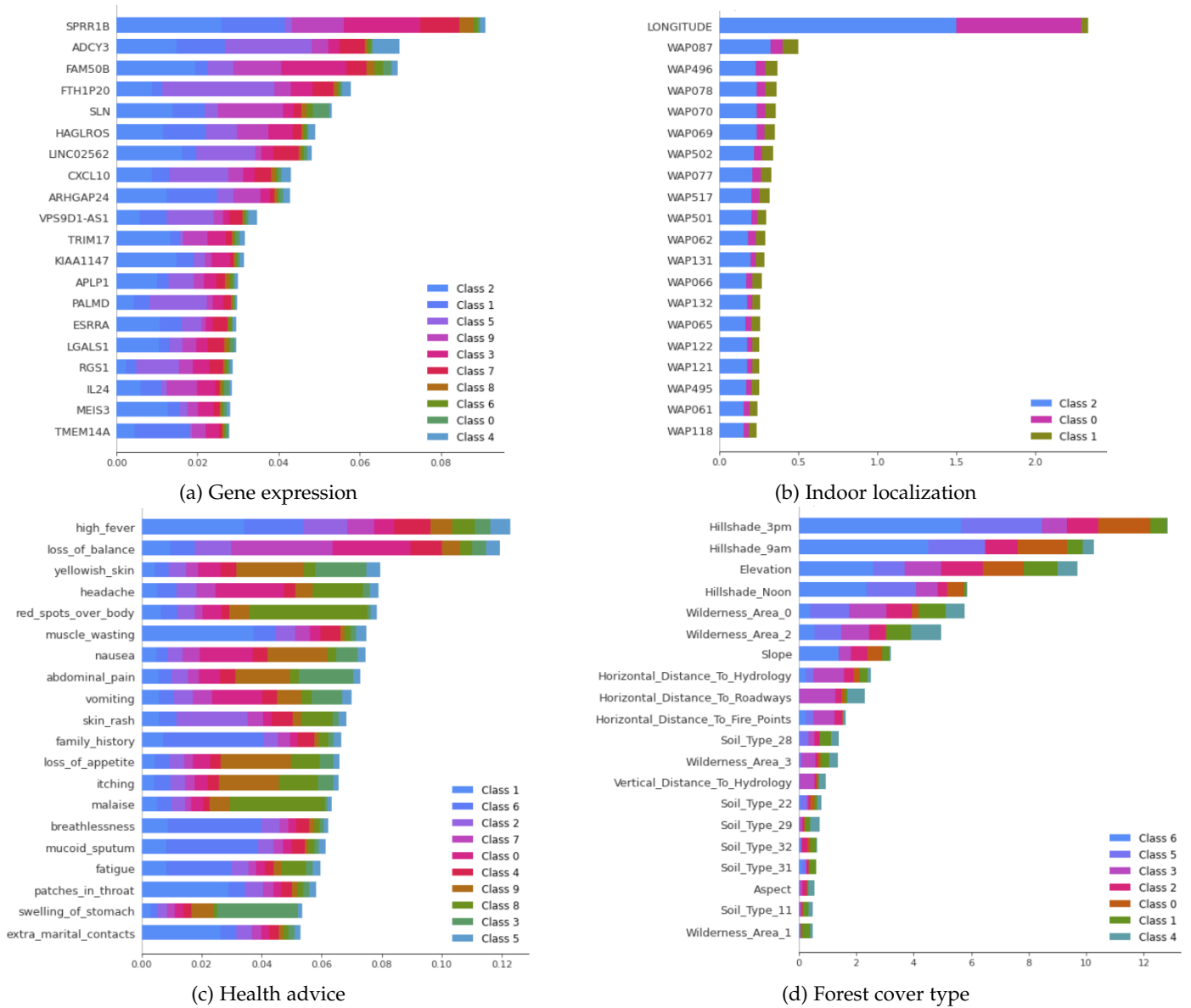


Fig. 11: Common features per class across datasets sorted from most to least w.r.t global feature importance



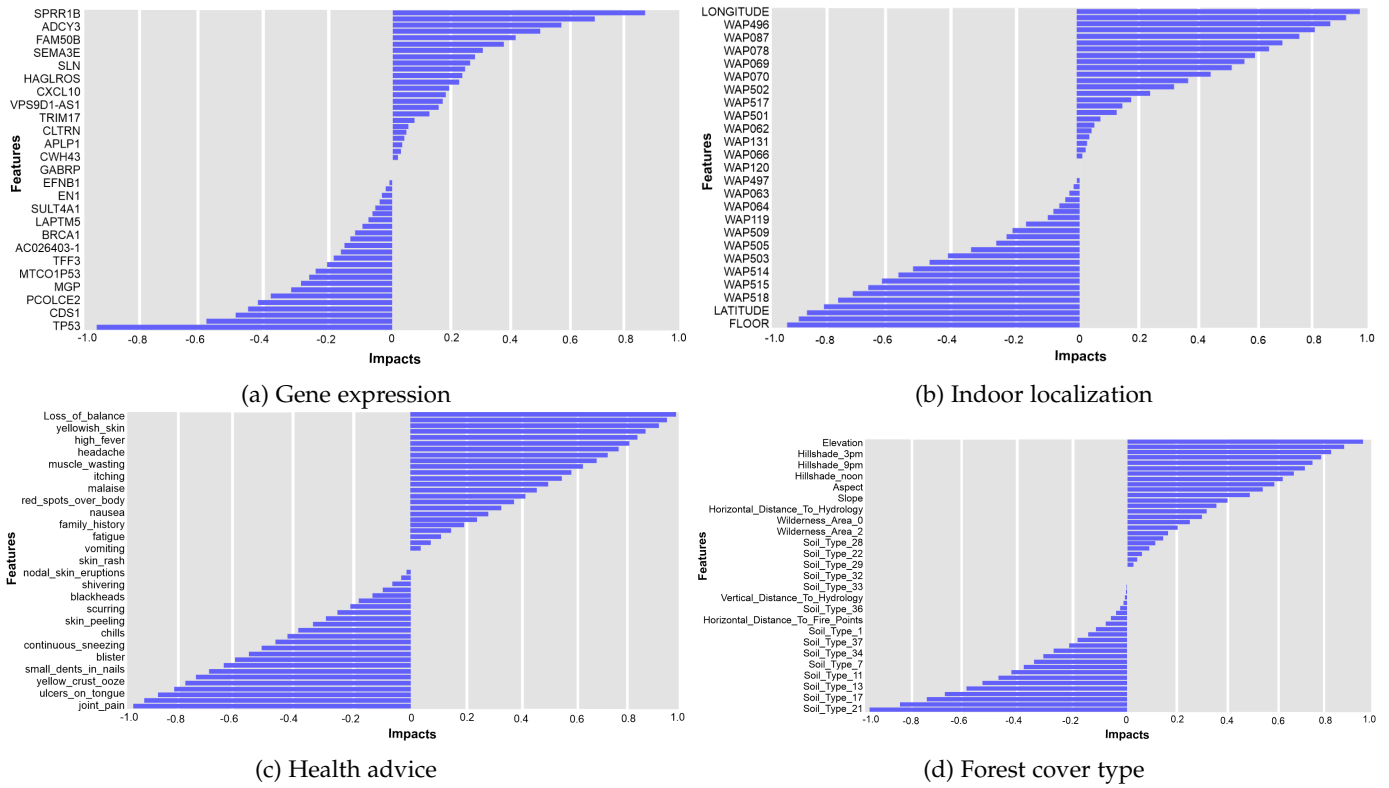


Fig. 12: Global feature impacts for the surrogate ERT model across datasets, sorted w.r.t SHAP value

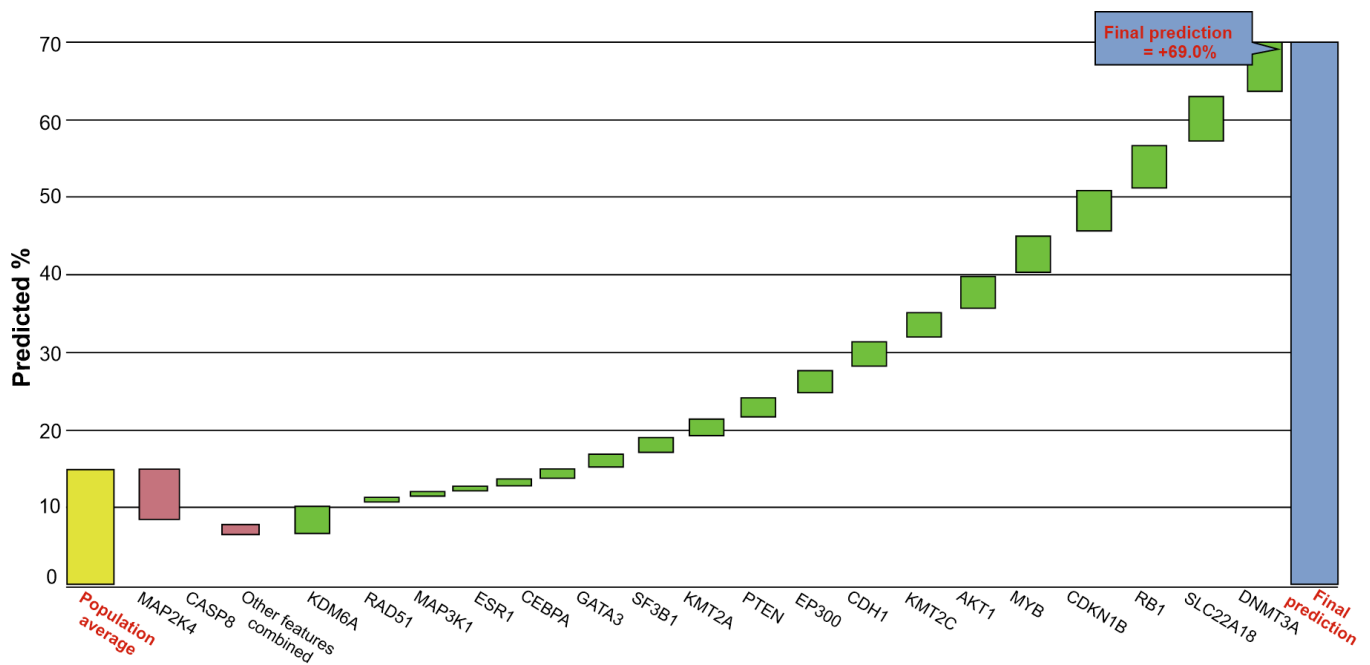


Fig. 13: Individual feature contribution for an observation

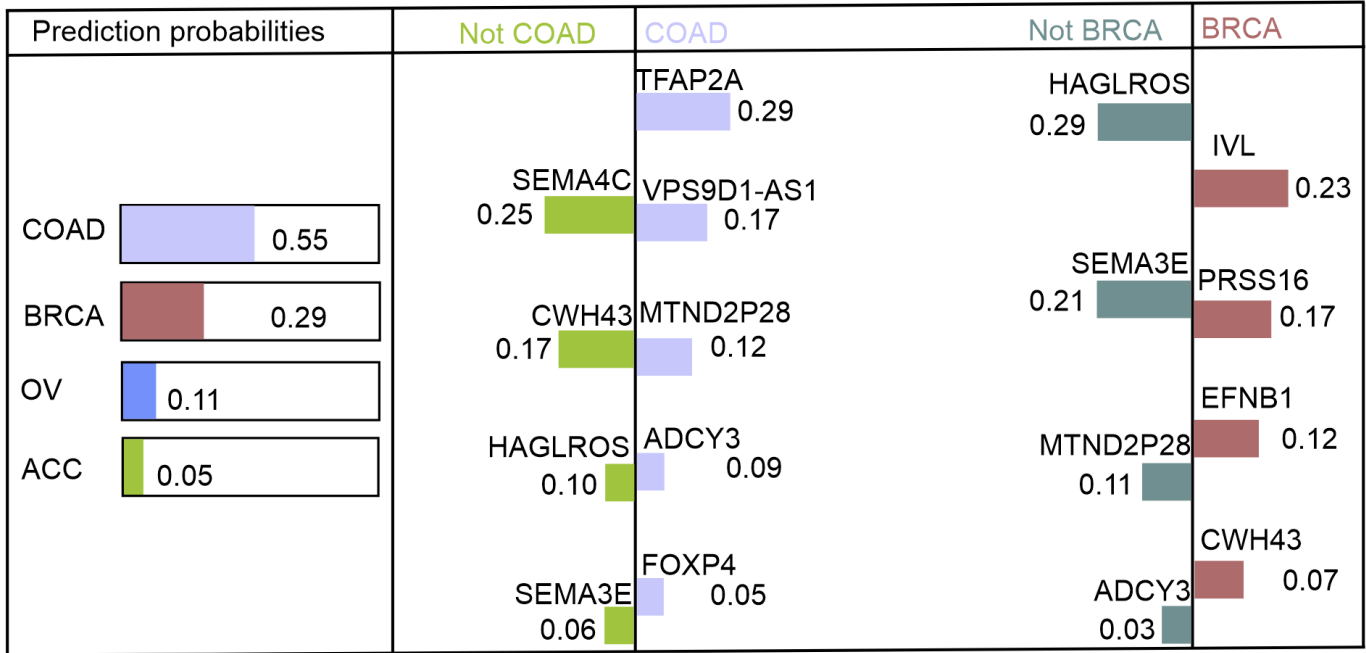
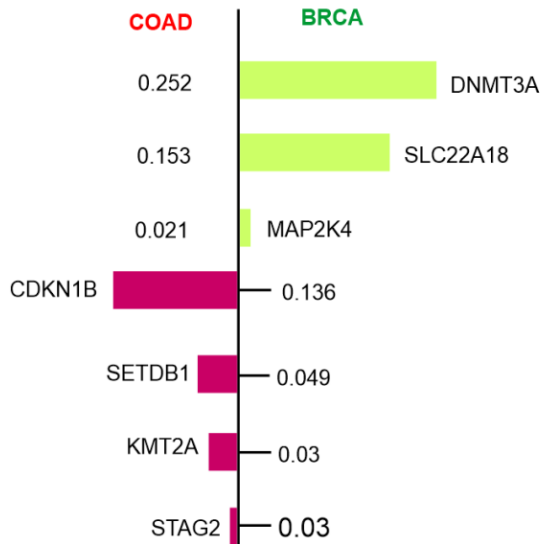


Fig. 14: Feature-level relevance for a single prediction

LORE:

$r = \{MAP2K4 \geq 8.23, EZH2 \geq 2.92, DNMT3A \geq 0.63, KMT2A < 0.77, CDKN1B < 0.47 \rightarrow decision = BRCA\}$   
 $\Phi = [\{DNMT3A \geq 0.63, KMT2A < 0.77, CDKN1B \leq 1.41, PTEN > 2.70, STAG2 > 2.24 \rightarrow decision = COAD\},$   
 $\{MYB \leq 1.08, KMT2C > 0.64, RUNX1 \leq 6.38, SLC22A18 \leq 6.43, PTEN > 2.70 \rightarrow decision = COAD\},$   
 $\{RUNX1 \leq 6.38, MYB > 0.058, FOXA1 \leq 3.35, KMT2A \leq 0.81, RB1 \leq 3.34 \rightarrow decision = COAD\}]$

LIME:



Anchor:

$r = (\{CDKN1B < 0.47, SETDB1 < 0.70, STAG2 < 3.29, PTEN > 2.70, CASP8 \leq 0.58\} \rightarrow decision = BRCA)$

Fig. 15: Explaining single prediction with rules and counterfactuals